Available online at www.sciencedirect.com
SCIENCE DIRECT®
Journal of Magnetic Resonance 174 (2005) 43–53
JMR Journal of Magnetic Resonance
www.elsevier.com/locate/jmr

Temperature dependence of protein backbone motion from carbonyl ^{13}C and amide ^{15}N NMR relaxation

Shou-Lin Chang, Nico Tjandra *

Laboratory of Biophysical Chemistry, Building 50, National Heart, Lung, and Blood Institute, National Institutes of Health, Bethesda, MD 20892, USA

Received 5 November 2004; revised 10 December 2004
Available online 10 February 2005

Abstract

The NMR spin–lattice relaxation rate (R_1) and the rotating-frame spin–lattice relaxation rate ($R_{1\rho}$) of amide ^{15}N and carbonyl ^{13}C ($^{13}C'$) of the uniformly ^{13}C- and ^{15}N-labeled ubiquitin were measured at different temperatures and field strengths to investigate the temperature dependence of overall rotational diffusion and local backbone motion. Correlation between the order parameter of the N–H vector, S^2_{NH}, and that of the carbonyl carbon, $S^2_{C'}$, was investigated. The effective $S^2_{C'}$ was estimated from the direct fit of the experimental relaxation rates and from the slope of $2R_2 - R_1$ vs. B^2 using Lipari–Szabo formalism. The average S^2_{NH} decreased by 5.9%, while the average $S^2_{C'}$ decreased by 4.6% from 15 to 47 °C. At the extreme low and high temperatures the difference in the temperature dependence of the order parameters vanishes. At the intermediate temperatures they do not change by the same amount but they follow the same trend. On the same peptide plane along the protein sequence, $S^2_{C'}$ and S^2_{NH} are highly correlated. The results suggest that fast local motion experienced at the site of the N–H vector and carbonyl nucleus is more complicated than previously thought and it cannot be easily described by one single type of motion in a broad range of temperature.
Published by Elsevier Inc.

Keywords: NMR relaxation; Carbonyl relaxation; Protein dynamics; Temperature dependence; Order parameters

1. Introduction

Nuclear magnetic resonance (NMR) is a powerful tool for elucidating molecular structure and dynamics. Detailed information about biological processes and molecular events can be extracted from the spin relaxations [1–7]. The fast ns–ps motion and slower ms–μs conformational exchange of the protein backbone are routinely investigated using ^{15}N relaxation. In general, spin nuclei other than ^{15}N such as carbonyl $^{13}C'$, amide ^{1}H, and $^{13}C_\alpha$ are potential candidates for probing backbone dynamics. However, severe spin diffusion from efficient dipolar interactions among the proton network complicates the interpretation of ^{1}H data [8,9]. In a fully ^{13}C- and ^{15}N-double-labeled protein accurate $^{13}C_\alpha$ relaxation rates are difficult to obtain due to homo-nuclear J coupling and cross-correlation interference from adjacent carbons [10]. Although the $^{13}C'$ relaxation involves several neighboring nuclei and complicated relaxation pathways, simplified interpretation can be constructed based on the dominant C' chemical shift anisotropy (CSA) term. Furthermore, the three-bond $^{3}J_{C'-C'}$ is relatively small and the impact of homo-nuclear isotropic mixing can be minimized by positioning the carrier frequency away from the center of the spectrum [11]. Several studies have appeared in the literature using auto-correlated carbonyl relaxation to investigate protein backbone motion in both the fast dynamics regime (picosecond to nanosecond) [12–17]

* Corresponding author. Fax: +1 301 402 3405.
E-mail address: nico@helix.nih.gov (N. Tjandra).

1090-7807/$ - see front matter. Published by Elsevier Inc.
doi:10.1016/j.jmr.2005.01.008

and slow dynamics regime (microsecond to millisecond) [11,18].

Recently there has been great interest in studying the asymmetric fast motion of the peptide plane [16,19–23]. Because the $^{13}C'$ CSA tensor has different orientation with respect to the N–H vector, experimental utilization of $^{13}C'$ relaxation in combination with ^{15}N relaxation has become popular for probing such asymmetry. Concurrently the Gaussian axial fluctuation (GAF) model has been proposed as a sophisticated motional model [22]. The GAF model offers a promising framework providing insight into the anisotropy of fast local motion. One observation from the GAF molecular dynamics (MD) simulation suggested that the largest angular fluctuation occurs along the σ_γ axis, that is, in the C^α_{i-1}–C^α_i direction. However, the qualitative and quantitative agreement between the GAF MD simulation and experimental NMR relaxation were not satisfactory as shown in the study of ubiquitin by Lienin et al. [16]. Furthermore, the fitted GAF parameters obtained by Carlomagno et al. [23] using cross-correlated relaxations suggested that in the case of ubiquitin, $\sigma_{\alpha\beta}$ was larger than σ_γ, which is a total contradiction to the results from Lienin et al., where auto-correlated relaxation rates were measured. Adopting a different approach, Wang et al. [19] addressed the asymmetry of motion by studying the temperature dependence of the effective order parameters of $^{13}C'$–$^{13}C_\alpha$ vector and ^{15}N–H vector derived from the auto-correlated, cross-correlated, and cross-relaxations involving ^{15}N, $^{13}C'$, and $^{13}C_\alpha$ nuclei. Based on the observation of the differential temperature dependence of the order parameters, they concluded that the $^{13}C'$–$^{13}C_\alpha$ vector experienced a larger motion than the ^{15}N–H vector. This result challenged the widely believed crane-shaft type of motion for backbone dynamics. Currently, there is no coherent representation of asymmetric motion in the peptide plane.

Sophisticated models and methodologies, in conjunction with accurate experimental data, will be eventually required to address the subtlety of these questions. In this study, we demonstrated that useful dynamics information can still be preserved through a simplified model-free approach. We measured temperature- and field-dependent ^{15}N and $^{13}C'$ auto-correlated relaxation rates and demonstrated that the effective carbonyl order parameter $S^2_{C'}$ can be estimated from the direct fit of relaxation rates and by the field-dependent $2R_2 - R_1$ value. We also investigated the correlation of $S^2_{C'}$ and S^2_{NH}. From there, the asymmetric motion of the peptide plane was addressed. Based on the temperature dependence of the order parameters at the site of N–H vector and carbonyl carbon, the fast motion exhibits small asymmetry at temperatures between 27 and 40 °C. At the very low and high temperatures the isotropic motions seem to dominate.

2. Materials and methods

2.1. Sample preparation

^{13}C- and ^{15}N-labeled ubiquitin was purchased from VLI Research (PA, USA). The sample for NMR relaxation studies contained 6 mg protein in 300 μl water with 5% D_2O and the final pH was adjusted to 4.75.

2.2. Measurement of the ^{15}N NMR R_1 and $R_{1\rho}$ relaxation rates

The NMR ^{15}N relaxation experiments at 15, 20, 27, 35, 40, and 47 °C were performed on a Bruker DRX 600 MHz spectrometer for the ^{13}C- and ^{15}N-labeled ubiquitin sample. The temperature for each measurement was calibrated by the chemical shift difference between the proton signal of HOD and the proton signal of 3-(trimethylsilyl)-1-propanesulfonic acid sodium salt (TSP). The spectrometer was equipped with a shielded x, y, z-pulsed-field gradient, triple resonance 5 mm probe. The States–TPPI quadrature detection in the t_1 dimension was used for all experiments. The ^{15}N and ^1H carrier frequencies were set to 116.5 ppm and the water frequency, respectively. The NMR data were processed using NMRPipe [24] and analyzed with PIPP software packages [25].

The standard R_1 and $R_{1\rho}$ pulse sequences [26] were modified to include WATERGATE solvent suppression [27], pulsed-field gradients, and a semi-constant time evolution period in t_1 [28]. $^{13}C_\alpha$ and $^{13}C'$ were decoupled during t_1 evolution by 180° pulses positioned at 56 and 177 ppm, respectively. A spin-lock field strength of 2500 Hz was applied for all $R_{1\rho}$ experiments. The $R_{1\rho}$ measurements with different relaxation delays were collected in an interleaved fashion. Each relaxation delay was sampled alternately every two scans. The cross-correlated effects were suppressed by 180° ^1H , $^{13}C'$, and $^{13}C_\alpha$ pulse trains during the relaxation period. Eight relaxation delays per experiment were chosen between 30 and 1300 ms for R_1 experiments and between 5 and 235 ms for $R_{1\rho}$ experiments. The relaxation time constants were calculated by fitting the delay-dependent peak intensities to an exponential decay curve using the Levenberg–Marquardt method [29]. The R_2 values were subsequently calculated from the corresponding $R_{1\rho}$, R_1, spin-lock field strength, and offset frequency. The uncertainty in the relaxation rate was estimated by using 300 Monte Carlo simulations [29].

2.3. Measurement of the ^{13}C-carbonyl carbon R_1 and $R_{1\rho}$ relaxation rates

Temperature-dependent $^{13}C'$ relaxation experiments were performed at 15, 20, 27, 35, 40, and 47 °C on a

Bruker Avance 800 and a DRX 600 MHz spectrometer. At 27 °C, extra relaxation datasets were acquired on a Bruker 500 and a 360 MHz spectrometer. The temperature was calibrated as described in the ^{15}N relaxation experiments. HNCO type pulse sequences (see supporting materials) were used with the evolution period t_1 on ^{13}C′ nuclei [11]. During the t_1 evolution, the protons were decoupled with WALTZ-16 scheme. The cross-correlated relaxations between ^{13}C′ CSA and ^{15}N–^{13}C′ or ^{1}H–^{13}C′ dipolar interaction were suppressed by ^{1}H and ^{15}N 180° pulses during the relaxation delay of R_1 experiment. For the $R_{1\rho}$ experiment, WALTZ was used to decouple ^{1}H throughout the evolution period and relaxation delay. The alignment of the nuclear spin magnetization with the effective field was achieved by adiabatic rotations using an amplitude and frequency modulated tanh/tan pulse [11,30,31]. The adiabatic ramps were 4 ms with a maximum field strength of 2500 Hz for experiments carried out at 14.1 T and 3333 Hz at 18.8 T. To minimize the effect of three-bond ^{13}C′–^{13}C′ J couplings, the offset of the carrier was temporarily shifted 750 and 1000 Hz down field for measurements at the spectrometer frequencies of 600 and 800 MHz, respectively, during the adiabatic ramps and the spin-lock period [11]. A ^{15}N 180° pulse was applied during the relaxation delay to suppress the N–H/C′ CSA cross-correlation effect. Spin-lock field strengths of 2500 and 3333 Hz were applied on ^{13}C′ for $R_{1\rho}$ measured at the 600- and 800-MHz spectrometer frequencies, respectively. Eight relaxation delays between 8 and 250 ms were chosen for each measured $R_{1\rho}$ and eight relaxation delays between 10 and 1800 ms were chosen for R_1. Relaxation times were determined by fitting the delay-dependent peak intensities to an exponential function using the Levenberg–Marquardt method [29]. R_2 values were calculated from the corresponding $R_{1\rho}$, R_1, spin-lock strength, and offset frequency. The error in the relaxation rate was estimated using 300 Monte Carlo simulations.

2.4. Calculation of overall correlation time τ_c

The overall rotational diffusion correlation time was determined using the ^{15}N relaxation R_2/R_1 ratio at 14 T as described previously [26,32]. Under the assumption of fast internal motion, this ratio is approximately independent of internal motion. For ^{13}C-, ^{15}N-labeled ubiquitin, the relaxations caused by the ^{15}N–C′ and the ^{15}N–C$_\alpha$ dipolar interaction must be taken into account. Although the ^{15}N–C′ and the ^{15}N–C$_\alpha$ vectors do not generally experience the same local motion as the ^{15}N–H vector does, the deviation introduced in the determination of τ_c by assuming a uniform order parameter is negligible. Residues with unusual R_2/R_1 values (deviation larger than 1.5 times standard of deviation) or R_2 field dependent, possibly due to chemical exchange, were excluded from the analysis [32]. The overall rotational diffusion of ubiquitin can be approximated as isotropic [32]. The isotropic assumption introduces approximately 0.6 and 10% deviation in the order parameter and deviation in the time constant compared to an axially symmetric model [32]. The correlation time was obtained by minimizing the target function E:

$$E = \sum_i \left(\frac{R_{2i}^{\exp}}{R_{1i}^{\exp}} - \frac{R_{2i}^{\mathrm{cal}}}{R_{1i}^{\mathrm{cal}}} \right)^2 \Big/ \sigma_i^2. \tag{1}$$

The index i in the equation represents the residue number; the upper index exp and cal represents experimental data and calculated relaxation rates; and σ represents the propagation of error in R_2/R_1. The error of the rotational diffusion coefficient was estimated from the standard deviation of twenty τ_c values that were calculated by randomly excluding ten R_2/R_1 points in the minimization. The S^2_{NH} and τ_f were then determined by fitting R_1 and R_2 values using the optimized τ_c.

The overall rotational diffusion constant can also be independently derived from ^{13}C′ R_1, and R_2 rates at two fields, which will be described in the following section.

2.5. Dynamics analysis of carbonyl carbon relaxation

The general expressions for CSA and dipolar (DD) contribution to the spin–lattice relaxation rate R_1, and the spin–spin relaxation rate R_2 for spin 1/2 nuclei are given below [33]:

$$R_1^{\mathrm{CSA}} = \frac{1}{T_1^{\mathrm{CSA}}} = \gamma_I^2 B_0^2 [g_2^{\mathrm{CS}}(\omega)], \tag{2}$$

$$R_2^{\mathrm{CSA}} = \frac{1}{T_2^{\mathrm{CSA}}} = \frac{1}{2}\gamma_I^2 B_0^2 \left[g_2^{\mathrm{CS}}(\omega) + \frac{4}{3} g_2^{\mathrm{CS}}(0) \right], \tag{3}$$

$$R_1^{\mathrm{DD}} = \frac{1}{T_1^{\mathrm{DD}}} = \gamma_I^2 \gamma_S^2 \hbar^2 \left[\frac{1}{3} g_2^D(\omega_I - \omega_S) + g_2^D(\omega_I) + 2 g_2^D(\omega_I + \omega_S) \right], \tag{4}$$

$$R_2^{\mathrm{DD}} = \frac{1}{T_2^{\mathrm{DD}}} = \frac{1}{2}\gamma_I^2 \gamma_S^2 \hbar^2 \left[\frac{4}{3} g_2^D(0) + \frac{1}{3} g_2^D(\omega_I - \omega_S) + g_2^D(\omega_I) + 2 g_2^D(\omega_S) + 2 g_2^D(\omega_I + \omega_S) \right], \tag{5}$$

where the function $g(\omega)$ is defined in Table 1 [33], $\hbar$ is Planck's constant divided by 2π, γ is the gyromagnetic ratio. The indices CSA and DD represent contribution from the chemical shift anisotropy and dipolar interaction, respectively. The equations in Table 1 describe the relaxation contribution of an asymmetric interac-

Table 1
The components of $g(\omega)$

l	K	τ_{lk}	c_{lk}
2	−2	$\frac{1}{6D_S}\left[1+\frac{D^*}{2D_S}\right]^{-1}$	$\frac{\delta_\lambda^2}{40}\{3\sin^2\beta\sin 2\gamma-\eta_\lambda[\cos 2\alpha\sin 2\gamma(\cos^2\beta+1)+2\sin 2\alpha\cos 2\gamma\cos\beta]\}^2$
2	−1	$\frac{1}{6D_S}\left[1-\frac{D^*}{4D_S}(1-\eta_D)\right]^{-1}$	$\frac{\delta_\lambda^2}{40}\{3\sin 2\beta\cos\gamma+\eta_\lambda[\cos 2\alpha\sin 2\beta\cos\gamma-2\sin 2\alpha\sin\beta\sin\gamma]\}^2$
2	0	$\frac{1}{6D_S}\left[1-\frac{D^*A}{2D_S}\right]^{-1}$	$\frac{\delta_\lambda^2}{60A(1+A)}\left\{\frac{3}{2}(1+A)(3\cos^2\beta-1-\eta_\lambda\sin^2\beta\cos 2\alpha)-\frac{\eta_D}{2}[3\sin^2\beta\cos 2\gamma-\eta_\lambda(\cos 2\alpha\cos 2\gamma(\cos^2\beta+1)-2\sin 2\alpha\sin 2\gamma\cos\beta)]\right\}^2$
2	1	$\frac{1}{6D_S}\left[1-\frac{D^*}{4D_S}(1+\eta_D)\right]^{-1}$	$\frac{\delta_\lambda^2}{40}\{3\sin 2\beta\sin\gamma+\eta_\lambda[\cos 2\alpha\sin 2\beta\sin\gamma+2\sin 2\alpha\sin\beta\cos\gamma]\}^2$
2	2	$\frac{1}{6D_S}\left[1+\frac{D^*A}{2D_S}\right]^{-1}$	$\frac{\delta_\lambda^2}{20A(1+A)}\left\{\frac{-\eta_D}{2}(3\cos^2\beta-1-\eta_\lambda\sin^2\beta\cos 2\alpha)+\frac{1+A}{2}[3\sin^2\beta\cos 2\gamma-\eta_\lambda(\cos 2\alpha\cos 2\gamma(\cos^2\beta+1)-2\sin 2\alpha\sin 2\gamma\cos\beta)]\right\}^2$

α, β, and γ are the eulerian angles transforming the interaction coordinate to the diffusion coordinate.
$D_S=\frac{1}{3}(D_{xx}+D_{yy}+D_{zz})$, $D^*=D_{zz}-D_S$, $\eta_D=\frac{D_{yy}-D_{xx}}{D^*}$; $\delta_\lambda=\sigma_{zz}$, $\eta_\lambda=\frac{\sigma_{yy}-\sigma_{xx}}{\sigma_{zz}}$ for CSA interaction; $\delta_\lambda=r_{ij}^{-3}$, $\eta_\lambda=0$ for dipolar interaction; $g_l(\omega)=\sum_{k=-l}^{l}\frac{c_{lk}\tau_{lk}}{1+\omega^2\tau_{lk}^2}$ no internal motion; $g_l(\omega)=\sum_{k=-l}^{l}c_{lk}\left\{\frac{S^2\tau_{lk}}{1+\omega^2\tau_{lk}^2}+\frac{(1-S^2)\tau_e}{1+\omega^2\tau_e^2}\right\}$, $\tau_e^{-1}=\tau_{lk}^{-1}+\tau_f^{-1}$ in the presence of internal motion.

tion tensor under an asymmetric overall rotational diffusion. The equations reduce to simpler forms when there is symmetry in the diffusion tensor or coupling tensor. For example, when the coupling tensor is axially symmetric, $\eta_\lambda=0$; when the diffusion tensor is axially symmetric, $\eta_D=0$ and $A=1$; and when the diffusion tensor is isotropic, $\eta_D=0$, $A=1$, and $D^*=0$.

For uniformly ^{13}C-, ^{15}N-double-labeled proteins, the relaxation rate of ^{13}C′ is the summation of the C′ CSA interaction, and dipolar interaction from nearby spins, such as C′–N, C′–C$_\alpha$, C′–Hs, etc.

$$R=R^{\mathrm{CSA}}+R^{\mathrm{DD,C'-N}}+R^{\mathrm{DD,C'-C_\alpha}}+\sum R^{\mathrm{DD,C'-H}}. \tag{6}$$

In our calculation, all protons within 6 Å to the ^{13}C′ atom were included. This essentially accounts for 99% of the dipolar contribution from protons in the protein according to our simulation based on a rotational diffusion correlation time of 5 ns at 14.1 T. A full analysis requires each interaction to have its own spectral density in order to describe the local motion. However, it is practically impossible to determine all the motional parameters from a limited number of experimental relaxation rates. Because the major contribution to the relaxation rates comes from the carbonyl CSA interaction by first order approximation, we apply an effective order parameter and correlation time to describe all interaction vectors.

The dynamics parameters were obtained by minimizing the target function E,

$$E=\sum_{i,j,k}\frac{(R_{ijk}^{\mathrm{cal}}-R_{ijk}^{\mathrm{exp}})^2}{\sigma_{ijk}^2}, \tag{7}$$

where R_{ijk}^{exp}, R_{ijk}^{cal}, and σ_{ijk} are the experimental relaxation rate, the theoretically calculated relaxation rate, and the standard deviation of relaxation rate i (R_1 and R_2) at field j for residue k. The parameters to be optimized are the overall correlation time τ_c, the order parameter S_k^2, and the internal correlation time $\tau_{f,k}$.

2.6. Isolation of CSA contribution from field-dependent $2R_2-R_1$ values

The value $2R_2-R_1$ can be calculated from Eqs. (2)–(5). The expression is shown in Eq. (8):

$$2R_2-R_1=\frac{4}{3}\gamma_I^2B_0^2g_2^{\mathrm{CS}}(0)+\sum_S\gamma_I^2\gamma_S^2\hbar^2\left[\frac{4}{3}g_2^D(0)+2g_2^D(\omega_S)\right], \tag{8}$$

where

$$g_2^{CS}(0) = \frac{3}{10}\left(\frac{2}{3}\Delta\right)^2\left(1+\frac{\eta_\lambda^2}{3}\right)\tau_c S^2, \quad (9)$$

$$\Delta = \sigma_{zz} - \frac{\sigma_{xx}+\sigma_{yy}}{2} = \frac{3}{2}\sigma_{zz}, \quad (10)$$

$$\eta_\lambda = \frac{\sigma_{yy}-\sigma_{xx}}{\sigma_{zz}}, \quad 0 \leqslant \eta_\lambda < 1, \quad (11)$$

and

$$g_2^D(\omega_S) = \frac{3}{10} r_{IS}^{-6} \frac{\tau_c S^2}{1+\omega^2\tau_c^2}. \quad (12)$$

The σ_{xx}, σ_{yy}, and σ_{zz} are the three principal components of the traceless C′ CSA tensor. The first term of Eq. (8) is the field-dependent CSA contribution at zero frequency and the second term contains small field dependence contributions from all the dipolar interactions. By neglecting the field dependence of the second term in the bracket, a plot of $2R_2 - R_1$ vs. the square of the field strength gives rise to a straight line with its slope proportional to the spectral density at zero frequency and the CSA tensor. The C′ order parameter can then be estimated if the overall correlation time and the CSA are available.

3. Result

3.1. Overall correlation times of ubiquitin

The overall correlation times of ubiquitin determined using ^{15}N R_2/R_1 ratio measured from the ^{13}C-, ^{15}N-labeled sample at 15, 20, 27, 35, 40, and 47 °C were estimated to be 5.40 ± 0.01, 4.80 ± 0.01, 4.02 ± 0.01, 3.41 ± 0.01, 3.05 ± 0.01, and 2.68 ± 0.01 ns, respectively (Fig. 1). The correlation time at 27 °C is consistent with the previously published result (4.09 ns) using ^{15}N-labeled protein [32]. It is important to note that slight inconsistencies in NMR sample conditions (such as pH, ionic strength, and/or residual solvent) can exist as a result of individual sample purification and preparation. These inconsistencies can potentially lead to undesirable effects when comparing NMR datasets acquired from two different samples. Therefore it is preferable to measure both ^{15}N and ^{13}C′ relaxation rates using the same double-labeled sample. Alternatively, τ_c can be obtained by analyzing ^{13}C′ R_1 and R_2 relaxation. However, using C′ R_2/R_1 ratio for determination of τ_c introduces significant errors when the internal motion has a time constant of around 50–100 ps, which is the case for our study. Engelke et al. [13] using a different approach reported a higher than average effective correlation time for ^{13}C′ around 350 ps. Our simulations indicated that at 14.1 T for $\tau_c = 4$ ns, $S^2 = 0.8$, and $\tau_f = 50$ ps, the ^{13}C′ R_2/R_1 approach introduced a 5% error, and for $\tau_f = 100$ ps a 10% error in R_2/R_1 ratio, while the ^{15}N R_2/R_1 approach only introduced a 3% error when $\tau_f = 100$ ps. Thus, for ^{13}C′ relaxation data, τ_c has to be optimized simultaneously with the internal motion parameters S^2 and τ_f. The τ_c values estimated from ^{13}C′ relaxation were 5.28 ± 0.01, 4.75 ± 0.01, 4.04 ± 0.01, 3.33 ± 0.01, 3.02 ± 0.01, and 2.70 ± 0.01 at 15, 20, 27, 35, 40 and 47 °C, respectively (Fig. 1). The overall correlation times that were calculated are in good agreement with each other from the two independent datasets and analysis.

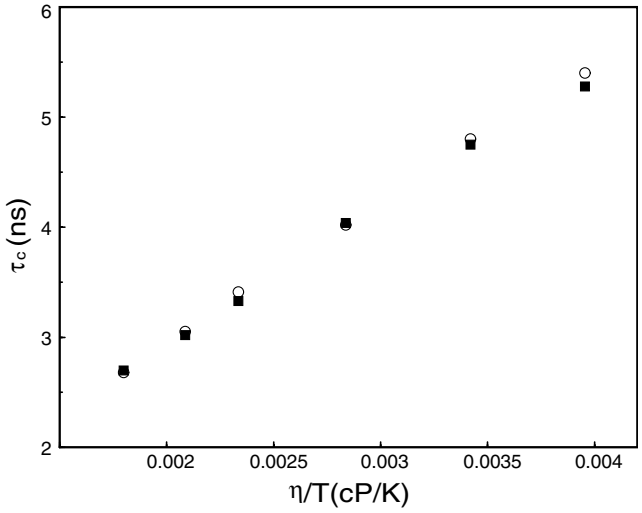

Fig. 1. Temperature dependence of isotropic overall correlation time τ_c of ubiquitin calculated from ^{15}N R_2/R_1 ratio (open circle) and from direct fit to ^{13}C R_1 and R_2 rates (filled square). An error of ±0.01 ns was estimated using Monte Carlo simulation.

3.2. Temperature dependence of N–H order parameters

The order parameters of N–H bonds were calculated from the R_1 and R_2 relaxation rates measured at 14.1 T using the double-labeled ubiquitin sample. The results from four temperatures are shown in Fig. 2A. The average order parameters S^2_{NH} were 0.807 ± 0.003, 0.795 ± 0.003, 0.775 ± 0.004, 0.778 ± 0.003, 0.776 ± 0.003, and 0.759 ± 0.004 at 15, 20, 27, 35, 40, and 47 °C, respectively. The uncertainties were estimated from 100 Monte Carlo simulations. A 5.9% drop in the average order parameter is observed over the 32 °C range. Average order parameters were calculated only for residues with a signal present in all datasets, including both ^{15}N and ^{13}C′ relaxation. Excluding C-terminal residues (residues 71–76), the average time constants were 38, 43, 40, 41, 31, and 37 ps at 15, 20, 27, 35, 40, and 47 °C, respectively.

3.3. Lipari–Szabo model-free analysis of carbonyl carbon relaxation

The C′ R_1 and R_2 relaxation rates were acquired at 15, 20, 27, 35, 40, and 47 °C and at 18.8 and 14.1 T.

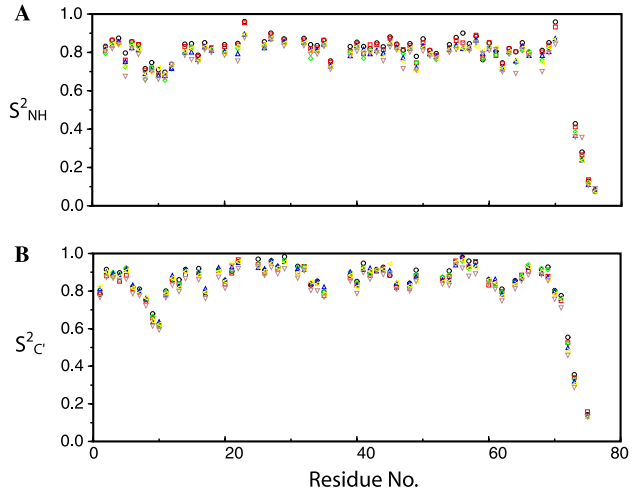

Fig. 2. Effective order parameters of N–H vector (A) and C′ (B). The circle, square, diamond, triangle up, triangle left, and triangle down denote order parameters at 15, 20, 27, 35, 40, and 47 °C, respectively.

Two parameters were used to describe the local motion of C′: one for the effective order parameter and one for the effective correlation time. The overall correlation time was optimized using a grid search approach. The values of the C′ CSA principal components (σ_{xx}, σ_{yy}, and σ_{zz}) and the angle (β), which is the angle of σ_{xx} axis relative to C–N bond on the peptide plane, were taken from solution NMR measurements [34], and were determined to be −74.7, −11.8, and 86.5 ppm and 38°, respectively. For molecules that undergo isotropic overall tumbling, the β angle has no effect on the contribution to the relaxation. The optimal overall correlation times were reported in the previous section. The calculated order parameters are shown in Fig. 2B. The average order parameters $S^2_{C'}$ were 0.848 ± 0.008, 0.835 ± 0.006, 0.842 ± 0.005, 0.844 ± 0.006, 0.836 ± 0.006, and 0.809 ± 0.007 at 15, 20, 27, 35, 40, and 47 °C, respectively. A 4.6% drop in order parameter was observed from 15 to 47 °C. The average time constants, excluding the protein tail (residues 71–75), were 80, 101, 74, 70, 76, and 63 ps at 15, 20, 27, 35, 40, and 47 °C, respectively. The time constant here is slightly larger than that of the N–H vector but not as large as reported in the study of Engelke et al. [13].

3.4. $^{13}C'$ order parameters estimated from field-dependent $2R_2 - R_1$

Simulation (with $\tau_c = 5$ ns, $S^2 = 0.8$, $\tau_f = 200$ ps at 14.1 T) indicates the average field-dependent dipolar contribution to the slope of $2R_2 - R_1$ vs. B^2 is less than 2% within the field range from 2.35 to 23.5 T (proton frequency from 100 MHz to 1 GHz). This guarantees the CSA $g(0)$ term obtained by estimating $2R_2 - R_1$ vs. B^2 is essentially "free" of a dipolar contribution. Further simplification can be made by dropping the fast motion term $(1 - S^2)\tau_f/(1 + \omega^2\tau_f^2)$, which contributes about 1% to the CSA $g(0)$. The remaining term in $g(0)$ is directly proportional to τ_c, $\Delta^2(1 + \eta^2/3)$, and S^2_C. Thus, a "pure" effective $S^2_{C'}$ can in turn be extracted, when the τ_c and CSA components are known. In practice, however, the slope of $2R_2 - R_1$ vs. B^2 determined from this approach is susceptible to the inconsistency of the experimental conditions for datasets acquired at different instruments. Note that the temperature detected at the sensor can deviate from the real temperature in the sample, especially for pulse sequences containing intensive continuous wave proton decoupling and ^{13}C spin-lock. This can be verified by calibrating the temperature using a TSP sample while switching on the decoupling and spin-lock pulses.

As a proof of concept, we first calculated the order parameter using only two fields of 14.1 and 18.8 T. The result (Fig. 3) shows a positive deviation in the order parameter obtained from direct fit to relaxation rates. This systematic error is likely due to a slightly higher than the expected temperature for the 600-MHz dataset or a slightly lower than the expected temperature for the 800-MHz dataset. That in turn gives a higher slope of $2R_2 - R_1$ vs. B^2, and hence a larger order parameter. By acquiring datasets at multiple fields, systematic errors of this kind can be reduced. When we incorporated two extra datasets from 8.5 and 11.7 T, the order parameters that were calculated became more consistent with the direct fit to relaxation rate result. Typical field-dependent $2R_2 - R_1$ is shown in Fig. 4. Residues undergoing conformational exchange will exhibit an unusually large slope as we found for residues E24 and E51, which were excluded from our analysis.

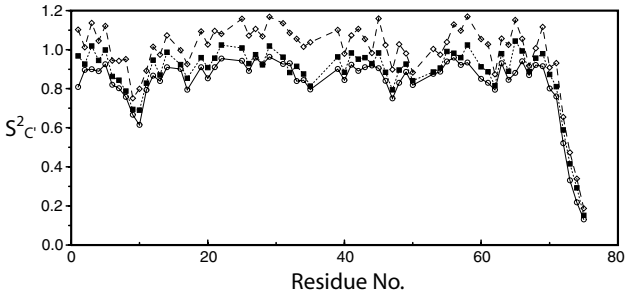

Fig. 3. Comparison of the carbonyl order parameters obtained from direct fit to relaxation rates and the order parameter from $2R_2 - R_1$ vs. B^2 approach. Open circle, order parameter from direct fit; open diamond, order parameter from $2R_2 - R_1$ vs. B^2 approach using two field strengths (14.1 and 18.8 T); and filled square, order parameter from $2R_2 - R_1$ vs. B^2 approach using four field strengths (8.5, 11.8, 14.1, and 18.8 T). The order parameters from two different approaches agree better when datasets from multiple field strengths are available for $2R_2 - R_1$ vs. B^2 approach.

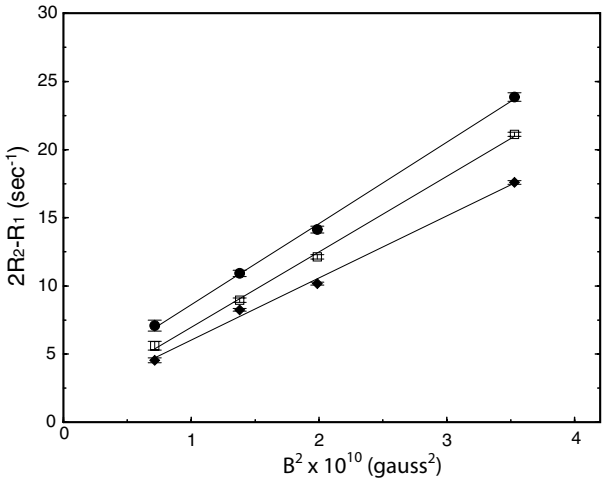

Fig. 4. Typical $2R_2 - R_1$ values as a function of B^2. Filled circle, K27; open square, G53; and filled diamond, T9. It is obvious from the figure that if the slope is determined only from two data points, the deviation can be very significant.

4. Discussion

4.1. The effect of $^3J_{C'C'}$ and $^3J_{C'C_\gamma}$ couplings on $T_{1\rho}$ in ubiquitin

Magnetization transfer through isotropic mixing caused by three-bond $^3J_{C'C'}$ and $^3J_{C'C_\gamma}$ coupling becomes efficient for near-degenerate resonances and for resonances positioned symmetrically with respect to the spin-lock frequency [11]. By moving the carrier frequency away from the center of the carbonyl dimension, the latter case can be circumvented [11]. In ubiquitin, neighboring residue pair A28–K29 at 15, 20, 27, 35, and 40 °C, and residue pair Q62–K63 at 15 and 20 °C have near-degenerate shifts (<0.1 ppm). Nevertheless, none of the four residues exhibits perceivable distorted relaxation curves resulting from Hartmann–Hahn matching. This can be explained by the relatively small $^3J_{C'C'}$ values within the helical and coiled region. The $^3J_{C'C'}$ constants for A28–K29 and Q62–K63 are unfortunately unavailable [35]. Of the five Asp residues (D21, D32, D39, D52, and D58) and two Asn residues (N25 and N60) that contain three-bond coupling $^3J_{C'C_\gamma}$, D58 at 15, 20, 27, and 35 °C displayed significant distortion due to isotropic mixing, and D21 at 15, 27, and 35 °C also displayed undesired effects. Both residues have a large $^3J_{C'C_\gamma}$ constant of 4.5 Hz [35]. Due to the change in the chemical shift difference between the carbonyl and carboxyl carbons under various temperatures, D21 and D58 did not suffer from the same effect throughout the whole temperature range. The residues subjected to strong isotropic mixing transfer were not excluded from our calculation of the average order parameter because the errors introduced by these residues can be neglected.

4.2. Correlation between $S^2_{C'}$ and S^2_{NH} and temperature dependence

The determination of $S^2_{C'}$ requires the knowledge of the $^{13}C'$ CSA tensor. The average orientation and the traceless components of the CSA tensor measured in solution [34,36,37] and in solid-state [38–43] have been reported. Our calculations were based on the average $^{13}C'$ CSA values estimated from residual chemical shifts reported by Cornilescu and Bax [34], where $\beta = 38°$, $\sigma_{xx} = -74.7$ ppm, $\sigma_{yy} = -11.8$ ppm, and $\sigma_{zz} = 86.5$ ppm. The choice of different average CSA values affects the absolute value of $S^2_{C'}$. The offset we observe between $S^2_{C'}$ and S^2_{NH} may be partly due to an underestimated CSA value or N–H bond length. The use of an average CSA value does not account for possible variation in individual residues that may be located in different secondary structures and involved in different hydrogen bonding pattern. Nevertheless, the correlation coefficients between the order parameter $S^2_{C'(n-1)}$ and $S^2_{NH(n)}$ on the same peptide plane along the protein sequence are significant, which are 0.95, 0.95, 0.95, 0.94, 0.92, and 0.91, at 15, 20, 27, 35, 40, and 47 °C, respectively. Considering the possible variation in CSA values $\Delta^2(1+\eta^2/3)$ along the sequence, the correlation here represents the "minimum" correlation. The correlation between $S^2_{C'(n-1)}$ and $S^2_{NH(n)}$ we observed here seems much better than what Engelke and Rueterjans found in their study on ribonuclease T_1 [13].

Alternatively, if we assume the motion of peptide plane is isotropic, meaning $S^2_{C'(n-1)}$ and $S^2_{NH(n)}$ are identical, the "maximum" percentage standard deviation of ^{13}C $\Delta^2(1+\eta^2/3)$ will be equal to the variation in the $S^2_{C'(n-1)}/S^2_{NH(n)}$ (or $S^2_{NH(n)}/S^2_{C'(n-1)}$) ratio along the sequence, which is about 7%. Using three cross-correlation measurements and an assumption that motion of the peptide plane is isotropic, Cisnetti et al. [37] calculated residue specific CSA components and orientation for ubiquitin. The percentage standard deviation of $\Delta^2(1+\eta^2/3)$ is about 13%, which is higher than our 7% based on the similar argument. It is significant that the effective order parameter used in their work was taken from measurements for N–H vectors [32].

Another factor that might contribute to the offset between $S^2_{C'(n-1)}$ and $S^2_{NH}(n)$ is the N–H bond length. A longer N–H bond results in a smaller dipolar contribution. The consequence is that smaller overall correlation times or larger internal order parameters are expected in order to fit the original experimental relaxation data. Since the overall rotational diffusion correlation times were determined by the ratio of T_1 and T_2, the effect of N–H bond length was insignificant due to a partial cancellation. Therefore, the variation of N–H bond length will mainly be absorbed by the internal motion parameters. By changing the length from 1.02 to 1.03 Å, at 15 °C, we observed slight changes in the

average fast correlation time, and the average S^2_{NH} will increase from 0.807 to 0.841, which is closer to the average $S^2_{C'}$.

Besides a high correlation between $S^2_{C'(n-1)}$ and $S^2_{NH(n)}$, both average $S^2_{C'}$ and S^2_{NH} decreased by comparable amounts, 5.9% for S^2_{NH} and 4.6% for $S^2_{C'}$ within the temperature range from 15 to 47 °C. The change of average order parameter from 20 to 47 °C, with respect to the order parameter at 15 °C, is given in Fig. 5. The difference in the order parameters from 15 to 40 °C is small. Despite the small range of the variation, two independently measured and analyzed datasets for two nuclei followed interestingly similar temperature dependence at the extremes of temperatures (20 and 47 °C). At the intermediate temperatures the $S^2_{C'}$ and S^2_{NH} did not show the same temperature dependence. This would suggest a more anisotropic motion in this range of temperature. However they have similar trend. We observed a smaller decrease in both order parameters at 35 °C relative to 27 and 40 °C. While at very low or high temperatures the amplitudes of the internal motions are scaled by the same factor, perhaps indicating a more isotropic motion. Our finding qualitatively agrees with the result found in the cross-correlated relaxation study by Wang et al. [19] over the temperature range between 15 and 35 °C. Both results show that $^{13}C'$ order parameter has different temperature dependence than ^{15}N order parameter. However quantitatively our data differ from Wang et al. While they found the $S^2_{C'}$ to decrease more rapidly than the S^2_{NH}, we found quite the opposite. Wang et al. measured cross-correlation and NOE rates that pertain predominantly to the motion of the C′–C_α vector, while our study report on the motion of the rhombic carbonyl CSA tensor which intermixes motions in the C′–C_α direction (σ_{xx}) with those of the N–H direction (σ_{yy}). Since there is no precedence to assume that the motions along these various directions are correlated, it is conceivable that the differences between the $S^2_{C'}$ and S^2_{NH} in the two studies may not be the same.

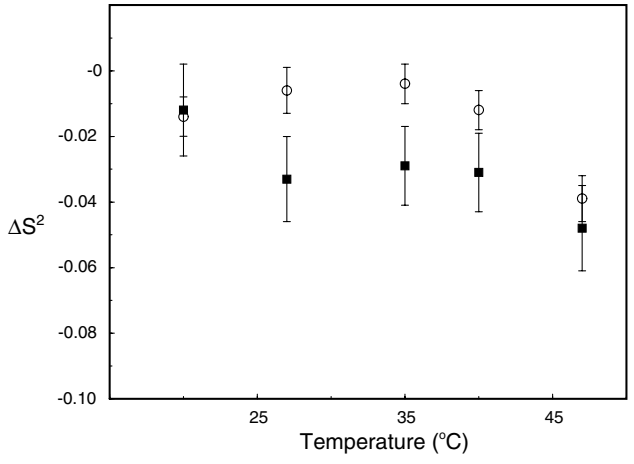

Fig. 5. Average order parameter changes as a function of temperature. The reference point is the order parameter at 15 °C. Filled square, N–H order parameter and open circle, carbonyl order parameter. The general trend is the order parameter decreases as temperature increases. The N–H and C′ order parameter decreased by 5.9 and 4.6% in the 32 °C range, respectively. In the region from 27 to 40 °C, a slight increase followed by a decrease in order parameter were observed for both N–H and C′.

Both studies however support the conclusion that the $^{13}C'$ relaxation reports on a differential temperature dependence of anisotropic motions of the peptide plane at the intermediate temperatures. It is of interest to note that Wang et al. [19] found the same effect for other small proteins. Interestingly we found that the difference between the two order parameters vanishes at higher temperature. This is indicative that more isotropic motions dominate at higher temperatures, at least for ubiquitin. These observations are of great importance to the modeling of fine details of local motion.

While interesting from the theoretical point of view, the mentioned motional anisotropy is small at all temperatures studied. Thus, it may be concluded that the ^{15}N and $^{13}C'$ relaxation measurements are in practice equally valid and good probes of local molecular dynamics. Importantly, we demonstrate a clear correlation between the order parameters found for $^{13}C'$ and ^{15}N. In contrast, the $^{13}C'$ cross-correlation measurements used by Wang et al., while precise, are not a very accurate indicators of dynamics on a site-by-site basis. This is most likely due to the fact that the $^{13}C'$–C_α cross-correlation rates are more sensitive to variations in the $^{13}C'$ tensor direction than the auto-correlation rates. Overall, it may thus be concluded that our approaches are the method of choice for the measurements over overall $^{13}C'$ dynamics; the methods of Wang et al. are of interest when studying the details of local motion.

4.3. Implications from the extraction of $S^2_{C'}$ using the $2R_2 - R_1$ vs. B^2 approach

We indicated that even slight inconsistency in temperature during the experiment for datasets measured at different fields can lead to significant errors in the estimate of the slope of $2R_2 - R_1$ vs. B^2. This kind of systematic error can be easily spotted by the observation that the intercept of the $2R_2 - R_1$ vs. B^2 curve becomes physically unreasonable, either with a large positive or even with a negative value. Note that the value of the intercept comes from the residual terms of dipolar contribution. The systematic error of this kind not only biases the absolute value but also introduces unpredictable deviation among the order parameters of the residues in the sequence. The error can be reduced by careful calibration, which is experimentally difficult when high power decoupling and spin-lock is present, or by incorporating datasets from as many fields as possible. As we have demonstrated, when the $2R_2 - R_1$ values at four fields were included, the order parameter

approached the value we obtained from direct fit to the relaxation rates. Since the slope of $2R_2 - R_1$ vs. B^2 curve is directly proportional to the product of the $\Delta^2(1 + \eta^2/3)$ term and the order parameter, the CSA components chosen for calculation will have a direct impact on the absolute value of $S^2_{C'}$. On average, the ratio $S^2_{C'}/S^2_{NH}$ we obtained was about 1.064, yielding a $S^2_{C'}$ value approximately 6.4% larger than S^2_{NH}. It is still unclear if such an offset is physically real. The offset is not due to the isotropic overall tumbling, because using an axially symmetric model will only introduce less than 1% deviation. However, as mentioned previously, deviation in the $\Delta^2(1 + \eta^2/3)$ term may significantly contribute to the offset. To remove the offset, the $\Delta^2(1 + \eta^2/3)$ term will have to be increased by 6.4%. Several studies on the magnitude of CSA components give variable range values of the $\Delta^2(1 + \eta^2/3)$ term. Taken the result from Cornilescu and Bax [34] as 1, the $\Delta^2(1 + \eta^2/3)$ term from Pang and Zuiderweg [36] is 0.704, from Stark et al. [43] is 0.930. In other words, when using the results from Pang and Stark, the offset in the $S^2_{C'}$ and S^2_{NH} will become even larger. The $\Delta^2(1 + \eta^2/3)$ value relative to Cornilescu's result from the study of Cisnetti et al. [37] using ubiquitin X-ray structure is 1.003 and using NMR structure is 1.012. The values from Cisnetti and co-workers are not suitable in our calculation because earlier published S^2_{NH} values for ubiquitin [32] were used to derive their CSA parameters, which would become a circular argument for us. However, it is interesting to note that higher $\Delta^2(1 + \eta^2/3)$ values were indeed obtained in their study under an isotropic assumption. From this aspect, the Cornilescu's result is more consistent with the view of an isotropic peptide plane motion, since it gives the least offset between $S^2_{C'}$ and S^2_{NH}. Interestingly, Markwich and Sattler [45] recently formulated a simple model for the carbonyl CSA based on the DFT NMR carbonyl shielding tensor calculations. According to their formulation, the average calculated value of $\Delta^2(1 + \eta^2/3)$ for ubiquitin increases by 4%, which will draw the values of the $S^2_{C'}$ and S^2_{NH} even closer. Residue specific CSA values obtained by the same method can also be applied to derive the $S^2_{C'}$. This however did not result in any apparent change in the correlation between $S^2_{C'}$ and S^2_{NH}.

It is also worth mentioning that either the CSA term or the order parameter can be extracted when the other is assumed as a priori knowledge. Therefore, cautions also have to be taken when methods based on field-dependent $2R_2 - R_1$ are used to estimate CSA values [44]. Systematic errors or large variation could be produced when there is inconsistency in the temperature for datasets from different instruments.

In this study we have limited ourselves to the analysis of order parameters. We also have chosen to use the simplest analysis possible. There are no fundamental reasons why a more complicated motional model, such as the GAF model cannot describe the temperature dependence of order parameters that we observed. The only practical limitation is the number and accuracy of the available data sets needed to quantitatively evaluate the model. Our result showed no clear dependence of τ_f on temperature for both ^{15}N and $^{13}C'$. So far there is no consensus in published results on the behavior of fast correlation times as a function of temperature. One challenging issues for better determination of τ_f is very accurate measurements of NOE values. This is already quite difficult to achieve for the $^1H^N$–^{15}N. It is even harder to obtain in the case of $^{13}C'$. In addition reported values as large as 350 ps for $^{13}C'$ τ_f points to the need for a better understanding of the physical nature of this parameter.

5. Conclusion

The C′ CSA is the dominant contributor to carbonyl relaxation. Using this dominant term, the C′ auto-correlated rate constants can be reasonably approximated and still retain all of the useful dynamical information. The simplest approach of using model-free formalism could still provide meaningful clues to possible amplitudes of motions at wide range of temperatures. We demonstrated that the effective order parameter $S^2_{C'}$ can be extracted using a direct fit to relaxation rates at two fields and by the $2R_2 - R_1$ vs. B^2 approach. Along the protein sequence, $S^2_{C'}$ is highly correlated with S^2_{NH}. The overall temperature dependence of these order parameters is small in the range of temperatures studied. Some of their features however could still be extracted. At very low and very high temperatures both order parameters have similar temperature dependence. This would indicate either the motions are different but they scale the same way as a function of temperature or the motions are isotropic. They show different dependence in the intermediate temperatures suggesting the presence of anisotropic motions. Our results hint at a more complicated peptide plane motions than what was previously proposed.

Appendix A. Supplementary data

Supplementary data associated with this article can be found, in the online version, at doi:10.1016/j.jmr.2005.01.008.

References

[1] M. Akke, R. Bruschweiler, A.G. Palmer III, NMR order parameters and free energy: An analytical approach and its application to cooperative Ca^{2+} binding by calbindin D9k, J. Am. Chem. Soc. 115 (1993) 9832–9833.

[2] D. Yang, Y.K. Mok, J.D. Forman-Kay, N.A. Farrow, L.E. Kay, Contributions to protein entropy and heat capacity from bond vector motions measured by NMR spin relaxation, J. Mol. Biol. 272 (1997) 790–804.
[3] D. Yang, L.E. Kay, Contributions to conformational entropy arising from bond vector fluctuations measured from NMR-derived order parameters: Application to protein folding, J. Mol. Biol. 263 (1996) 369–382.
[4] A.L. Lee, A.J. Wand, Microscopic origins of entropy, heat capacity and the glass transition in proteins, Nature 411 (2001) 501–504.
[5] L. Spyracopoulos, P. Lavigne, M.P. Crump, S.M. Gagne, C.M. Kay, B.D. Sykes, Temperature dependence of dynamics and thermodynamics of the regulatory domain of human cardiac troponin C, Biochemistry 40 (2001) 12541–12551.
[6] S.-L. Chang, A. Szabo, N. Tjandra, Temperature dependence of domain motions of calmodulin probed by NMR relaxation at multiple fields, J. Am. Chem. Soc. 125 (2003) 11379–11384.
[7] J.J. Prompers, R. Bruschweiler, General framework for studying the dynamics of folded and nonfolded proteins by NMR relaxation spectroscopy and MD simulation, J. Am. Chem. Soc. 124 (2002) 4522–4534.
[8] A. Kalk, H.J.C. Berendsen, Proton magnetic relaxation and spin diffusion in proteins, J. Magn. Reson. 24 (1976) 343–366.
[9] T.S. Ulmer, I.D. Campbell, J. Boyd, Amide proton relaxation measurements employing a highly deuterated protein, J. Magn. Reson. 166 (2004) 190–201.
[10] T. Yamazaki, R. Muhandiram, L.E. Kay, NMR experiments for the measurement of carbon relaxation properties in highly enriched uniformly ^{13}C, ^{15}N-labeled proteins: Application to $^{13}C_{\alpha}$ carbons, J. Am. Chem. Soc. 116 (1994) 8266–8278.
[11] F.A.A. Mulder, M. Akke, Carbonyl ^{13}C transverse relaxation measurements to sample protein backbone dynamics, Magn. Reson. Chem. 41 (2003) 853–865.
[12] K.T. Dayie, G. Wagner, Carbonyl-carbon relaxation rates reveal a dynamic heterogeneity of the polypeptide backbone in villin 14T, J. Magn. Reson. Series B 109 (1995) 105–108.
[13] J. Engelke, H. Ruterjans, Backbone dynamics of proteins derived from carbonyl carbon relaxation times at 500, 600 and 800 MHz: Application to ribonuclease T1, J. Biomol. NMR 9 (1997) 63–78.
[14] K.T. Dayie, G. Wagner, Carbonyl carbon probe of local mobility in ^{13}C, ^{15}N-enriched proteins using high-resolution nuclear magnetic resonance, J. Am. Chem. Soc. 119 (1997) 7797–7806.
[15] P. Allard, T. Hard, NMR relaxation mechanisms for backbone carbonyl carbons in a ^{13}C, ^{15}N-labeled protein, J. Magn. Reson. 126 (1997) 48–57.
[16] S.F. Lienin, T. Bremi, B. Brutscher, R. Bruschweiler, R.R. Ernst, Anisotropic intramolecular backbone dynamics of ubiquitin characterized by NMR relaxation and MD computer simulation, J. Am. Chem. Soc. 120 (1998) 9870–9879.
[17] K. Huang, R. Ghose, J.M. Flanagan, J.H. Prestegard, Backbone dynamics of the N-terminal domain in *E. coli* DnaJ determined by ^{15}N- and ^{13}CO-relaxation measurements, Biochemistry 38 (1999) 10567–10577.
[18] R. Ishima, J. Baber, J.M. Louis, D.A. Torchia, Carbonyl carbon transverse relaxation dispersion measurements and ms–μs time-scale motion in a protein hydrogen bond network, J. Biomol. NMR 29 (2) (2004) 187–198.
[19] T. Wang, S. Cai, E.R. Zuiderweg, Temperature dependence of anisotropic protein backbone dynamics, J. Am. Chem. Soc. 125 (28) (2003) 8639–8643.
[20] Y. Pang, M. Buck, E.R. Zuiderweg, Backbone dynamics of the ribonuclease kinase active site area using multinuclear (^{15}N and ^{13}CO) NMR relaxation and computational molecular dynamics, Biochemistry 41 (2002) 2655–2666.
[21] D. Idiyatullin, I. Nesmelova, V.A. Daragan, K.H. Mayo, Comparison of $^{13}C_{\alpha}H$ and ^{15}NH backbone dynamics in protein GB1, Protein Sci. 12 (2003) 914–922.
[22] T. Bremi, R. Bruschweiler, Locally anisotropic internal polypeptide backbone dynamics by NMR relaxation, J. Am. Chem. Soc. 119 (1997) 6672–6673.
[23] T. Carlomagno, M. Maurer, M. Hennig, C. Griesinger, Ubiquitin backbone motion studies via NH–C′Cα dipolar–dipolar and C′–C′Cα/NH CSA-dipolar cross-correlated relaxation, J. Am. Chem. Soc. 122 (2000) 5105–5113.
[24] F. Delaglio, S. Grzesiek, G.W. Vuister, G. Zhu, J. Pfeifer, A. Bax, NMRPipe: A multidimensional spectral processing system based on UNIX pipes, J. Biomol. NMR 6 (1995) 277–293.
[25] D.S. Garrett, R. Powers, A.M. Gronenborn, G.M. Clore, A common-sense approach to peak picking in 2-dimensional, 3-dimensional, and 4-dimensional spectra using automatic computer-analysis of contour diagrams, J. Magn. Reson. 95 (1991) 214–220.
[26] L.E. Kay, D.A. Torchia, A. Bax, Backbone dynamics of proteins as studied by ^{15}N inverse detected heteronuclear NMR spectroscopy: Application to staphylococcal nuclease, Biochemistry 28 (1989) 8972–8979.
[27] M. Piotto, V. Saudek, V. Sklenar, Gradient-tailored excitation for single-quantum NMR spectroscopy of aqueous solutions, J. Biomol. NMR 2 (1992) 661–665.
[28] S. Grzesiek, A. Bax, Amino acid type determination in the sequential assignment procedure of uniformly $^{13}C/^{15}N$-enriched proteins, J. Biomol. NMR 3 (1993) 185–204.
[29] W.H. Press, S.A. Teukolsky, W.T. Vetterling, B.P. Flannery, Numerical Recipes in C, second ed., Cambridge Press, 1999.
[30] F.A.A. Mulder, R.A. de Graff, R. Kaptein, R. Boelens, An off-resonance rotating frame relaxation experiment for the investigation of macromolecular dynamics using adiabatic rotations, J. Magn. Reson. 131 (1998) 351–357.
[31] M. Garwood, Y. Ke, Symmetric pulses to induce arbitrary flip angles with compensation for RF inhomogeneity and resonance offsets, J. Magn. Reson. 94 (1991) 511–525.
[32] N. Tjandra, S.E. Feller, R.W. Pastor, A. Bax, Rotational diffusion anisotropy of human ubiquitin from ^{15}N NMR relaxation, J. Am. Chem. Soc. 117 (1995) 12562–12566.
[33] H.W. Spiess, Rotation of Molecules and Nuclear Spin Relaxation. ed., vol. 15, Springer-Verlag, Berlin, Heidelberg, New York, 1978.
[34] G. Cornilescu, A. Bax, Measurement of proton, nitrogen and carbonyl chemical shielding anisotropies in a protein dissolved in a dilute liquid crystalline phase, J. Am. Chem. Soc. 122 (2002) 10143–10154.
[35] J.-S. Hu, A. Bax, Measurement of three-bond $^{13}C–^{13}C$ J couplings between carbonyl and carbonyl/carboxyl carbons in isotopically enriched proteins, J. Am. Chem. Soc. 118 (1996) 8170–8171.
[36] Y. Pang, E.R. Zuiderweg, Determination of protein backbone ^{13}CO chemical shift anisotropy tensors in solution, J. Am. Chem. Soc. 122 (2000) 4841–4842.
[37] F. Cisnetti, K. Loth, P. Pelupessy, G. Bodenhausen, Determination of chemical shift anisotropy tensors of carbonyl nuclei in proteins through cross-correlated relaxation in NMR, ChemPhysChem 5 (2004) 807–814.
[38] M.D. Lumsden, R.E. Wasylishen, K. Eichele, M. Schindler, G.H. Penner, W.P. Power, R.D. Curtis, Carbonyl carbon and nitrogen chemical shift tensors of the amide fragment of acetanilide and *n*-methylacetanilide, J. Am. Chem. Soc. 116 (1994) 1403–1413.
[39] Y. Wei, D.-K. Lee, A. Ramamoorthy, Solid-state ^{13}C NMR chemical shift anisotropy tensors of polypeptide, J. Am. Chem. Soc. 123 (2001) 6118–6126.
[40] Q. Teng, M. Iqbal, T.A. Cross, Determination of the ^{13}C chemical shift and ^{14}N electric field gradient tensor orientations with respect to the molecular frame in a polypeptide, J. Am. Chem. Soc. 114 (1992) 5312–5321.

[41] T.G. Oas, C.J. Hartzell, T.J. McMahon, G.P. Drobny, F.W. Dahlquist, The carbonyl ^{13}C chemical shift tensors of five peptides determined from ^{15}N dipole-coupled chemical shift powder patterns, J. Am. Chem. Soc. 109 (1987) 5956–5962.
[42] N. Asakawa, M. Takenoiri, D. Sato, M. Sakurai, Y. Inoue, ^{13}C chemical shift tensors and secondary structure of poly-L-alanine by solid-state two-dimensional spin-echo NMR and ab initio chemical shielding calculation, Magn. Reson. Chem. 37 (1999) 303–311.
[43] R.E. Stark, L.W. Jelinski, D.J. Ruben, D.A. Torchia, R.G. Griffin, ^{13}C chemical shift and ^{13}C-^{15}N dipolar tensors for the peptide bond: [1-^{13}C Glycyl] ^{15}N glycine •HCl •H_2O, J. Magn. Reson. 55 (1983) 266–273.
[44] D. Fushman, N. Tjandra, D. Cowburn, An approach to direct determination of protein dynamics from ^{15}N NMR relaxation at multiple fields, independent of variable ^{15}N chemical Shift anisotropy and chemical exchange contributions, J. Am. Chem. Soc. 121 (1999) 8577–8582.
[45] P.R.L. Markwick, M. Sattler, Site-specific variations of carbonyl chemical shift anisotropies in proteins, J. Am. Chem. Soc. 126 (2004) 11424–11425.